




Evaluation of (η^6 -*p*-cymene) ruthenium diclofenac complex as anticancer chemotherapeutic agent: interaction with biomolecules, cytotoxicity assays

Rais Ahmad Khan, Hamad A. Al-Lohedan, Mohammad Abul Farah, Mohd Sajid Ali, Ali Alsalmeh, Khalid Mashay Al-Anazi & Sartaj Tabassum


To cite this article: Rais Ahmad Khan, Hamad A. Al-Lohedan, Mohammad Abul Farah, Mohd Sajid Ali, Ali Alsalmeh, Khalid Mashay Al-Anazi & Sartaj Tabassum (2019) Evaluation of (η^6 -*p*-cymene) ruthenium diclofenac complex as anticancer chemotherapeutic agent: interaction with biomolecules, cytotoxicity assays, Journal of Biomolecular Structure and Dynamics, 37:15, 3905-3913, DOI: [10.1080/07391102.2018.1528180](https://doi.org/10.1080/07391102.2018.1528180)


To link to this article: <https://doi.org/10.1080/07391102.2018.1528180>

 View supplementary material 

 Accepted author version posted online: 26 Sep 2018.
Published online: 24 Dec 2018.

 Submit your article to this journal 

 Article views: 199

 View related articles 

 View Crossmark data 



Evaluation of (η^6 -*p*-cymene) ruthenium diclofenac complex as anticancer chemotherapeutic agent: interaction with biomolecules, cytotoxicity assays

Rais Ahmad Khan^a, Hamad A. Al-Lohedan^b, Mohammad Abul Farah^c, Mohd Sajid Ali^b, Ali Alsalmeh^a, Khalid Mashay Al-Anazi^c and Sartaj Tabassum^b

^aDepartment of Chemistry, College of Sciences, King Saud University, Riyadh, KSA; ^bSurfactant Research Chair, King Saud University, Riyadh, KSA; ^cDepartment of Zoology, College of Sciences, King Saud University, Riyadh, KSA

Communicated by Ramaswamy H. Sarma

ABSTRACT

The designing of metal-based anticancer therapeutic agents can be optimized in a better and rapid way if the ligands utilized have standalone properties. Therefore, even when the organometallic/coordination complex (i.e., metallodrug) gets dissociated in extreme conditions, the ligand can endorse its biological properties. Herein, we have synthesized and characterized η^6 -*p*-cymene ruthenium diclofenac complex. Furthermore, the ruthenium complex interactions with human serum albumin (HSA) and ct-DNA have been studied using various spectroscopic studies viz., UV, fluorescence, and circular dichroism and exhibited a significant binding propensity. Furthermore, *in vitro* cytotoxicity assays were carried out against human breast cancer “MCF-7” cell line. The η^6 -*p*-cymene ruthenium diclofenac complex registered significant cytotoxicity with an IC_{50} value of $\sim 25.0 \mu\text{M}$ which is comparable to the standard drugs. The η^6 -*p*-cymene ruthenium diclofenac complex was able to decrease the MCF-7 cell proliferation and induced significant levels of apoptosis with relatively low toxicity.

ARTICLE HISTORY

Received 24 April 2018
Accepted 20 September 2018

KEYWORDS

Ruthenium diclofenac complex; biomolecular interaction; cytotoxicity against MCF7; apoptosis

1. Introduction

Metallo-chemotherapeutics is a well-established conventional selection for a wide range of diseases since ancient times, particularly for antibacterial, antifungal, analgesic, antipyretic, and anticancer. After the serendipitous discovery of cisplatin and its derivatives (Rosenberg, Van Camp, Grimley, & Thomson, 1967; Rosenberg, VanCamp, Trosko, & Mansour, 1969; Rosenberg, 1977, 1978), the field of metal-based chemotherapeutics got triggered, and since then, the field is evolved stalwartly. However, the acquired, intrinsic resistance and adverse side effects have marred the remarkable success of platinum-based drug candidates (Barry & Sadler, 2013; Galanski, Arion, Jakupec, & Keppler, 2003; Gasser & Metzler-Nolte 2012; Hill & Speer, 1982; Kelland, 2007; Khan et al., 2014).

In lieu of the problem of undesirable side effects and to improve efficacy, ruthenium complexes emerged as the potential class of anticancer agents. Among the Ru(III) compounds, NAMI-A (a metastasis agent) (imidazolium *trans*-[tetrachlorido(dimethyl sulfoxide (DMSO))(1H-imidazole) ruthenate (III)] and KP1019 (indazolium *trans*-[tetrachloridobis(1H-indazole)ruthenate(III)] and KP1339 (sodium (indazolium *trans*-[tetrachloridobis(1H-indazole)ruthenate(III)] exhibited potential activity against human tumor models, which are subjected to phase II clinical trials (Hartinger, Metzler-Nolte, & Dyson, 2012; Hartinger 2006, 2008). In recent decades, fluxional

ruthenium arene complexes have emerged as versatile scaffolds for the design of the new metallodrugs (Mehta, Gajera, & Patel, 2017; Yadav & Singh, 2018; Yuan, Zhang, Zheng, & Wang, 2013). In this area of half sandwich-organoruthenium, groups of scientist viz., Sadler et al. (Zhang & Sadler, 2017; Bruijninx & Sadler, 2009), Dyson et al. (Nazarov, Hartinger, & Dyson, 2014; Murray, Babak, Hartinger, & Dyson, 2016), and Keppler et al. (Hartinger et al., 2006; Renfrew et al., 2009) with their co-workers have marked a tremendous success with piano-stool-type geometry. RAPTA-C [$(\eta^6$ -*p*-cymene)Ru(PTA)Cl₂], PTA; 1,3,5-triaza-7-phosphatrimethyldecane and RM175 [Ru(η^6 -biphenyl)(ethylene-diamine)Cl]⁺ are the representatives of this class and hit the clinical trials with good impact. Merely having slight modifications in the structures of the two, they exhibited extremely different biological properties. These lead molecular frameworks have been extensively modified at both the ends viz., arenes part as well as the co-ligand/s to build up a structural-activity relationship (SAR) and decorated with different functionalities to get target specificity of the drug candidates.

Interestingly, combination therapy has also emerged in scientist who are working on the already existing drugs mainly nonsteroidal anti-inflammatory drugs (NSAIDs) and combining with the metal centers and studying the synergistic effect of metallodrugs, which have shown significant potential. In organo-ruthenium complexes, Turel et al. (Hudej

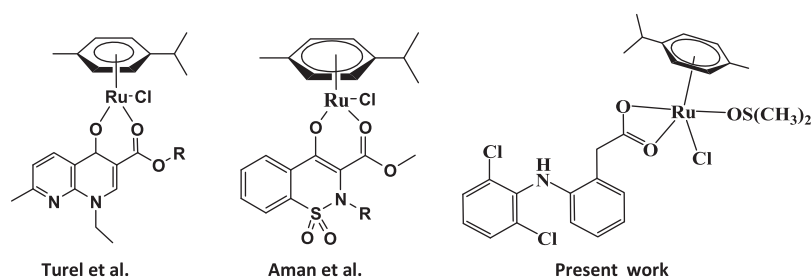


Figure 1. Structures of the representatives of this class of η^6 -*p*-cymene ruthenium complexes.



Figure 2. Schematic representation of the (η^6 -*p*-cymene) ruthenium complex of diclofenac (1).

et al., 2012; Kljun et al., 2011; Turel et al., 2010) synthesized Ru(arene) complexes of antibacterial compounds viz., nalidixic acid, ofloxacin. Likewise, Aman et al. (2014) have developed ruthenium arene compounds with oxicam moieties namely piroxicam and meloxicam (see Figure 1).

Thus, standing on this, we have studied the η^6 -*p*-cymene ruthenium-derived diclofenac complex (1) as a potential metallo-chemotherapeutic agent. The binding affinity of ruthenium complex with DNA and human serum albumin (HSA) has also been studied using various spectroscopic techniques and calculating various binding parameters. Furthermore, this ruthenium complex was studied against MCF-7 human breast cancer cell lines via cytotoxicity assays, studying the apoptotic potential and morphological changes induced by the potential metallodrug.

2. Experimental section

2.1. Materials and methods

The sodium salt of ct-DNA (D1501, Type I, fibers) and HSA essentially fatty acid free ($\geq 98\%$) were purchased from Sigma-Aldrich, St. Louis, MO. Tris(hydroxymethyl)aminomethane hydrochloride (Tris-HCl) was of analytical grade and also obtained from Sigma. Fetal bovine serum (FBS), trypsin/EDTA, and penicillin–streptomycin were purchased from Invitrogen (Carlsbad, CA). Trypan blue, phosphate buffered saline (PBS), dimethyl sulfoxide (DMSO), ethidium bromide, acridine orange, and Dulbecco's Modified Eagle's medium (DMEM) were obtained from Sigma-Aldrich (St. Louis, MO). Cell Titer 96[®] Non-radioactive cell proliferation assay kit was obtained from Promega (Madison, WI). Annexin V-FITC apoptosis detection kit was purchased from BD Biosciences (San Diego, CA). Culture wares and other consumables used in this study were procured from Nunc, Roskilde, Denmark.

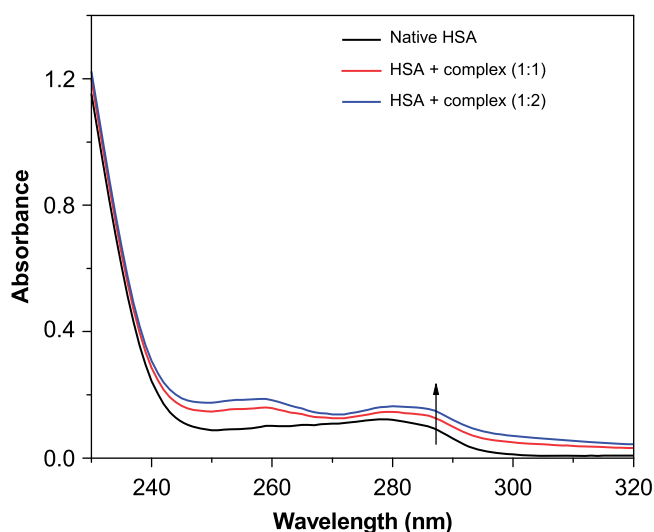


Figure 3. Difference UV-visible spectra of HSA-complex binding. [HSA] = 3 μ M.

2.2. Biological studies

2.2.1. HSA binding studies

HSA binding studies were carried out using UV-visible (UV-vis), fluorescence quenching, and circular dichroism methods, and the detailed experimental procedures for these studies have been described elsewhere (Afzal, Al-Lohedan, Usman, & Tabassum, 2018; Alsalmeh et al., 2016; Mach, Volkin, Burke, & Middaugh, 1995; Tabassum et al., 2017; Yousuf, Bashir, Arjmand, & Tabassum, 2018).

2.2.2. DNA binding studies

UV-vis spectroscopy, in the range of 225–350 nm, was used to understand the binding of η^6 -*p*-cymene ruthenium diclofenac complex (1) with DNA. Increasing concentration of ct-DNA was titrated against 30×10^{-6} mol dm⁻³ of η^6 -*p*-cymene ruthenium diclofenac complex. A fixed amount of ct-

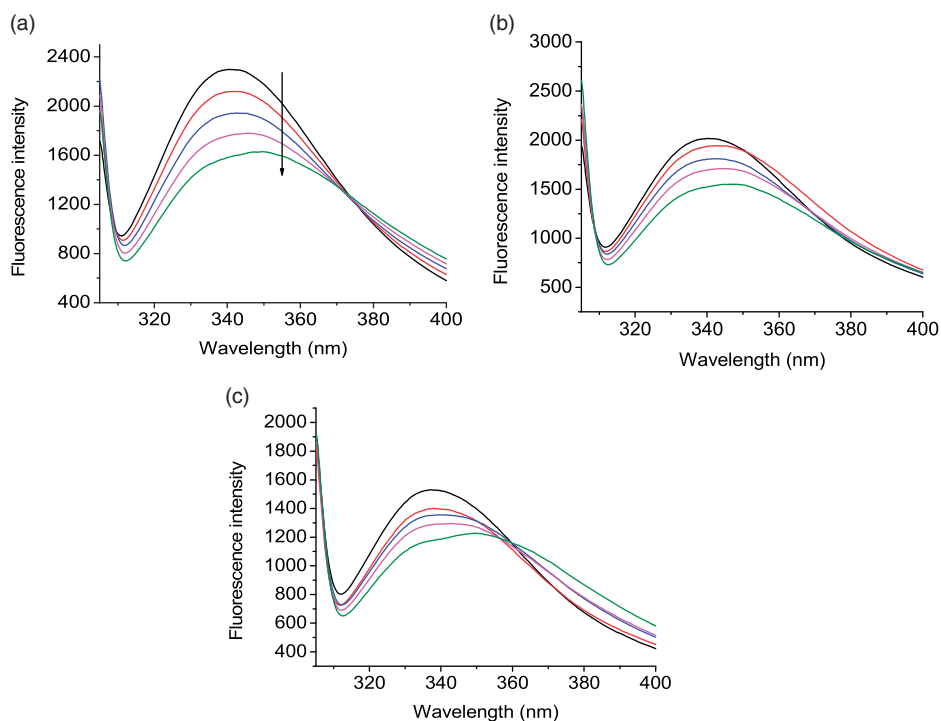


Figure 4. Effect of complex **1** on the fluorescence emission spectra ($\lambda_{\text{ex}} = 295 \text{ nm}$) of HSA at (a) 25, (b) 35, and (c) 45 °C. [HSA] = 3 μM , [complex] = 0, 2.5, 5, 7.5, 10 μM .

DNA ($0\text{--}30 \times 10^{-6} \text{ mol dm}^{-3}$) was taken in the blank, and baseline was corrected before each measurement. The binding mode of the $\eta^6\text{-}p\text{-cymene}$ ruthenium diclofenac complex was seen by competitive binding assay using EtBr and DAPI dyes. The circular dichroism studies of ct-DNA in the presence of complex were carried out similarly as described in the case of HSA binding (Afzal et al., 2018; Khan, Yadav, Hussain, Arjmand, & Tabassum, 2014; Mach et al., 1995; Tabassum et al., 2012; Yousuf et al., 2018).

2.2.3. Cell cultures, and in vitro cytotoxicity, apoptosis experiments

The MCF-7 human breast cancer cell culture, cytotoxicity, and apoptosis experiments were carried out by using standard protocols as adopted by Farah et al. (2016) with slight modifications; for more details, see [Supplementary information](#).

3. Result and discussion

3.1. Synthesis and characterization

To synthesize the ruthenium $\eta^6\text{-arene}$ NSAID compound (**1**), the sodium salt of diclofenac reacted with ($\eta^6\text{-}p\text{-cymene}$) ruthenium dichloride dimer was stirred in dry methanol and few drops of DMSO. The mixture was stirred at 80 °C for 10 h, and the reaction mixture kept on slow evaporation. The yellow color precipitation in yield of 68% was obtained. Unfortunately, after several attempts, we are unable to grow suitable single crystals for X-ray study. However, the ruthenium compounds synthesized were characterized by several

spectroscopic and analytical methods. Stability in aqueous medium and DMSO is an essential requirement for drug candidates, since DMSO/water was used to make a stock solution for biological studies. The ruthenium compound was found to be quite stable in DMSO while in H_2O , the chlorine atom gets hydrolyzed and forms an aqua complex of ruthenium over a period of 1 h (Figure 2).

The FT-IR spectrum of the complex **1** showed $\nu_{\text{asym}}(\text{C-O})$ and $\nu_{\text{sym}}(\text{C-O})$ at 1567 and 1459 cm^{-1} , respectively, which is characteristic for the bidentate coordination of carboxylate group of the ligand with a metal center. The difference between [$\nu_{\text{asym}}(\text{CO}) - \nu_{\text{sym}}(\text{CO})$] is 108 cm^{-1} , which is less than 150 cm^{-1} and thus confirms the bidentate binding mode of the carboxylate moiety. The FT-IR spectrum exhibited absorption band at 1157, 976, and 908 cm^{-1} , exhibiting a significant shift in $\nu(\text{S-O})$ corresponding to free DMSO (1005 cm^{-1}). Thus ascertains the coordination of DMSO through sulfur to the metal center. The band at 438 cm^{-1} is attributed to the $\nu(\text{Ru-O})$ (see Figure S1, [electronic Supplementary information](#)).

The proton nuclear magnetic resonance ($^1\text{H NMR}$) of complex **1** in DMSO-d_6 resulted in significant shifts when compared to the ligand. Complexation with ligand is confirmed by the disappearance of the carboxylic O-H signal from 10.27 ppm and the appearance of the $p\text{-cymene}$ proton additional signals. An upfield shift of the signals of 0.7–0.5 ppm of the ligand was observed in the ligand upon complexation. The band associated with the DMSO coordinated with the metal center and in solution due to the dissociation of the labile chlorido which is also quite evident and which leads to the formation of a most stable product which is ascertained

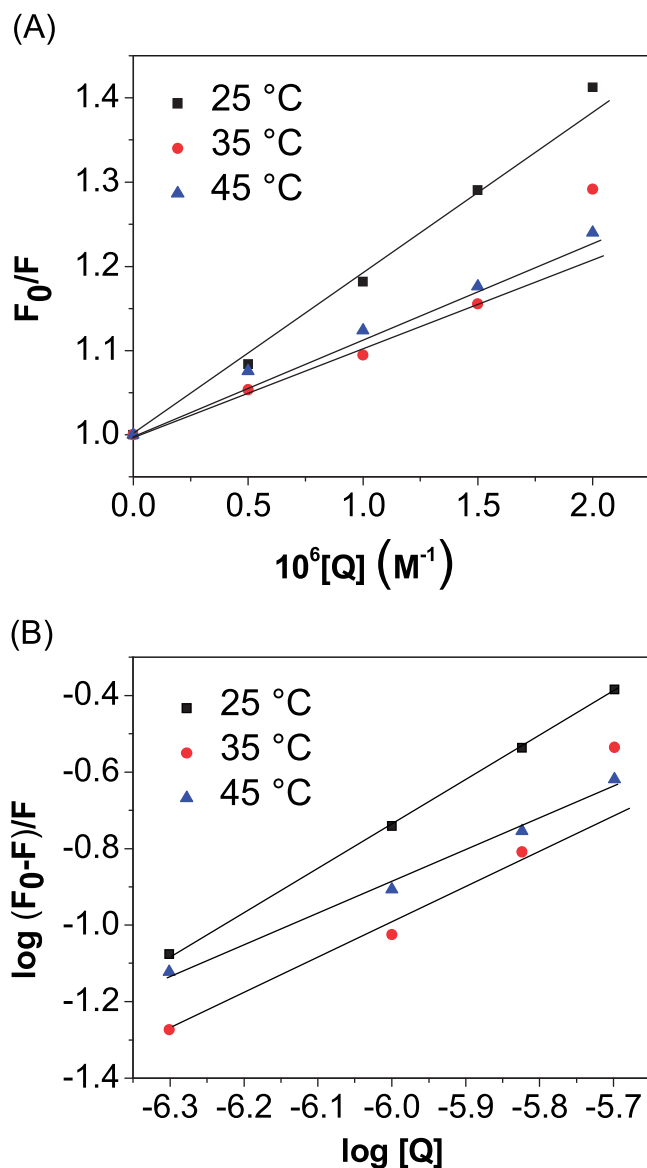


Figure 5. (a) Stern–Volmer plots of HSA interaction with complex 1 at various temperatures. [HSA] = 3 μM , λ_{ex} = 295 nm. (b) Plot of $\log(F_0 - F)/F$ as a function of \log [complex]. [HSA] = 3 μM , λ_{ex} = 295 nm.

by the electrospray ionization mass spectrometry (ESI-MS) of the complex (see Figures S2–S6, [Supplementary information](#)).

The UV–vis spectrum of the ligand exhibited the band at around ~ 275 nm ($n-\pi^*$ transition), and upon complexation, complex 1 displayed the band complex at ~ 260 nm with a significant shift of around 15 cm^{-1} and the new band appears at 323 nm (LMCT band) which confirms the coordination. The emission spectrum of the ruthenium complex was also taken in solution and found to exhibit signals at ~ 360 nm (see Figures S8 and S9, [Supplementary information](#)).

3.2. Biological studies

3.2.1. HSA binding studies

The difference UV–vis spectra of HSA with various concentrations of complex 1 are shown in [Figure 3](#).

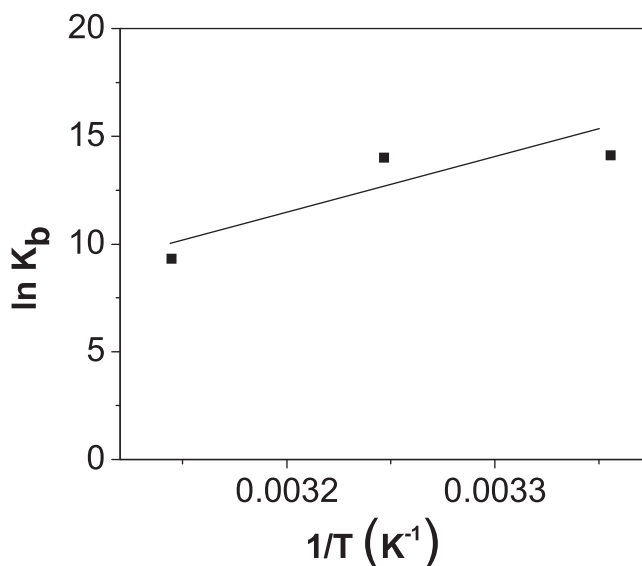


Figure 6. Van't Hoff plot of HSA interaction with complex 1. [HSA] = 3 μM , λ_{ex} = 295 nm.

HSA gives a peak at 280 nm which can be used to see the changes during its binding with the ligand (Mach et al., 1995). The increased intensity of the protein–Ru–diclofenac system in comparison to the pure HSA is an indication of the complex formation between HSA and Ru–diclofenac; moreover, a noticeable red shift of the absorption maximum is due to the involvement of electrostatic interaction.

The fluorescence intensity of HSA decreases gradually (Ali & Al-Lohedan, 2013, 2017) with the increase in the concentration of Ru–diclofenac complex ([Figure 4](#)). Since there is a significant red shift of about 11 nm in the maximum fluorescence emission at a wavelength, the involvement of electrostatic interactions has been proposed (Mandeville, Froehlich, & Tajmir-Riahi, 2009).

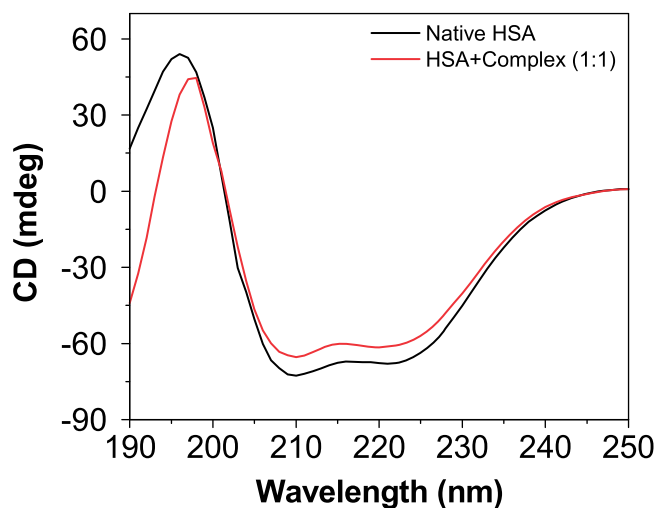
Various fluorescence and binding parameters have been calculated using [Figures 5 and 6](#) and Equations (S1)–(S3) (for equations, see [Supplementary information](#)), and their values are summarized in [Table 1](#) (Anand, Jash, & Mukherjee, 2010; Lakowicz, 1999).

A decreasing trend of the Stern–Volmer constant demonstrates the involvement of the static type of quenching mechanism. Binding parameters were computed using Equation (3) and [Figure 5\(b\)](#), and the data are displayed in [Table 1](#). There was approximately 1:1 binding between HSA and complex 1. The thermodynamic parameters (change in enthalpy (ΔH), entropy (ΔS), and free energy change (ΔG)) were calculated adopting the widely used Van't Hoff equation (Usman et al., 2017), for which the plot is given in [Figure 6](#).

The values of thermodynamic parameters, calculated by Equations (S4) and (S5) (for equations, see [Supplementary information](#)) using [Figure 6](#), are given in [Table 1](#), and it is clear from the negative values of ΔG that the binding of complex 1 with HSA is a spontaneous process. The interaction is also a highly exothermic process with a substantial ordering of the system as revealed by the negative values of both ΔH and ΔS .

Table 1. Stern–Volmer quenching constants, binding parameters, and thermodynamic parameters for the interaction of HSA with complex **1** at various temperatures.

T (K)	Stern–Volmer quenching constants			Binding parameters			Thermodynamic parameters		
	K_{sv} (M^{-1})	K_q ($M^{-1}s^{-1}$)	R^2	n	K (M^{-1})	R^2	ΔG ($KJ\ mol^{-1}$)	ΔH ($KJ\ mol^{-1}$)	ΔS ($J\ mol^{-1}\ K^{-1}$)
288	1.97×10^5	3.45×10^{13}	0.9924	1.1	13.6×10^5	0.9996	−36.87	−187.27	−504.69
298	1.25×10^5	2.19×10^{13}	0.9247	1.1	12.0×10^5	0.9529	−31.82		
308	1.20×10^5	2.10×10^{13}	0.9921	0.9	1.1×10^5	0.9921	−26.78		

 $\lambda_{ex} = 295\ nm.$

Figure 7. Far-UV CD spectra of HSA in the presence of complex **1** at 25 °C and pH 7.4. [HSA] = 3 μ M.

The far-UV CD is a useful method to determine the secondary structure of proteins (Ali & Al-Lohedan, 2016). The far-UV CD spectra of HSA in the absence and presence of complex **1** are given in Figure 7.

It is exhibited from the figure that the ellipticity of HSA is decreasing in the presence of the complex. Hence, it can be deduced that HSA partially unfolds in the presence of complex **1** (Feng, Lin, Yang, Wang, & Bai, 1998).

3.2.2. DNA binding studies

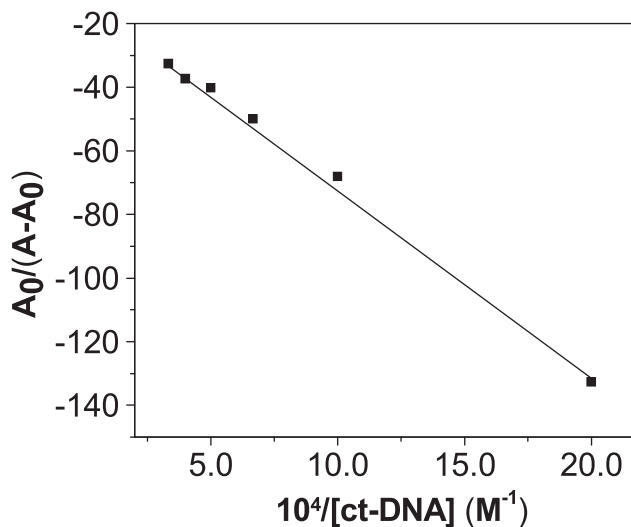
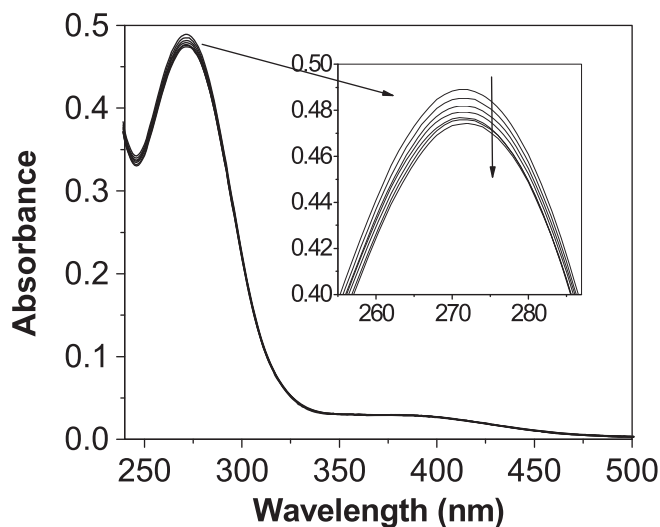
UV–vis spectroscopy is an important technique to obtain the information about ligand–biomolecule interactions. Difference UV–vis spectra of ct-DNA and complex **1** interaction are given in Figure 8. The addition of ct-DNA to complex **1** causes slight hypochromism in the spectra.

The changes in the absorbance at 278 nm were utilized to calculate the apparent association constant, K_{app} , of **1** and ct-DNA interaction

$$\frac{1}{A_{obs} - A_0} = \frac{1}{A_c - A_0} + \frac{1}{K_{app}(A_c - A_0)[ct - DNA]} \quad (1)$$

A graph of $1/(A_{obs} - A_0)$ versus $1/[ct-DNA]$ yielded a Benesi–Hildebrand (B–H) plot with a slope equal to $1/K_{app}(A_c - A_0)$ and an intercept equal to $1/(A_c - A_0)$. From the plot, the values of K_{app} were found to be $1.85 \times 10^4\ M^{-1}$.

From the collective information obtained from the DAPI and EtBr displacement assays (Figure 9), it is proposed that complex **1** is bound at the interfacial region of minor groove and intercalation site.


Figure 8. (a) UV–visible absorption spectra of ct-DNA (30 μ M) in the presence of increasing concentrations of complex **1** (0–30.0 μ M) at 25 °C. (b) Benesi–Hildebrand plot.

3.2.3. Cytotoxicity assay

The percent viability of cells is exposed to different concentrations of complex **1** and ruthenium dimer (**R**) (5.0–50.0 μ M). The IC_{50} value estimated at 24 h post treatment in MCF-7 for complex **1** is about 25.0 μ M and for **R** is \sim 400 μ M. A significant ($p < 0.05$) decrease in the cell viability was observed which was also concentration dependent. At the highest concentration of 50.0 μ M, cell proliferation was inhibited by 77 and 59% with complex **1** and **R** (ruthenium salt) treatment, respectively. While at the lowest concentration of 5.0 μ M, 79 and 88% cell growths were registered for complex **1** and **R** treatment, respectively. These data suggest

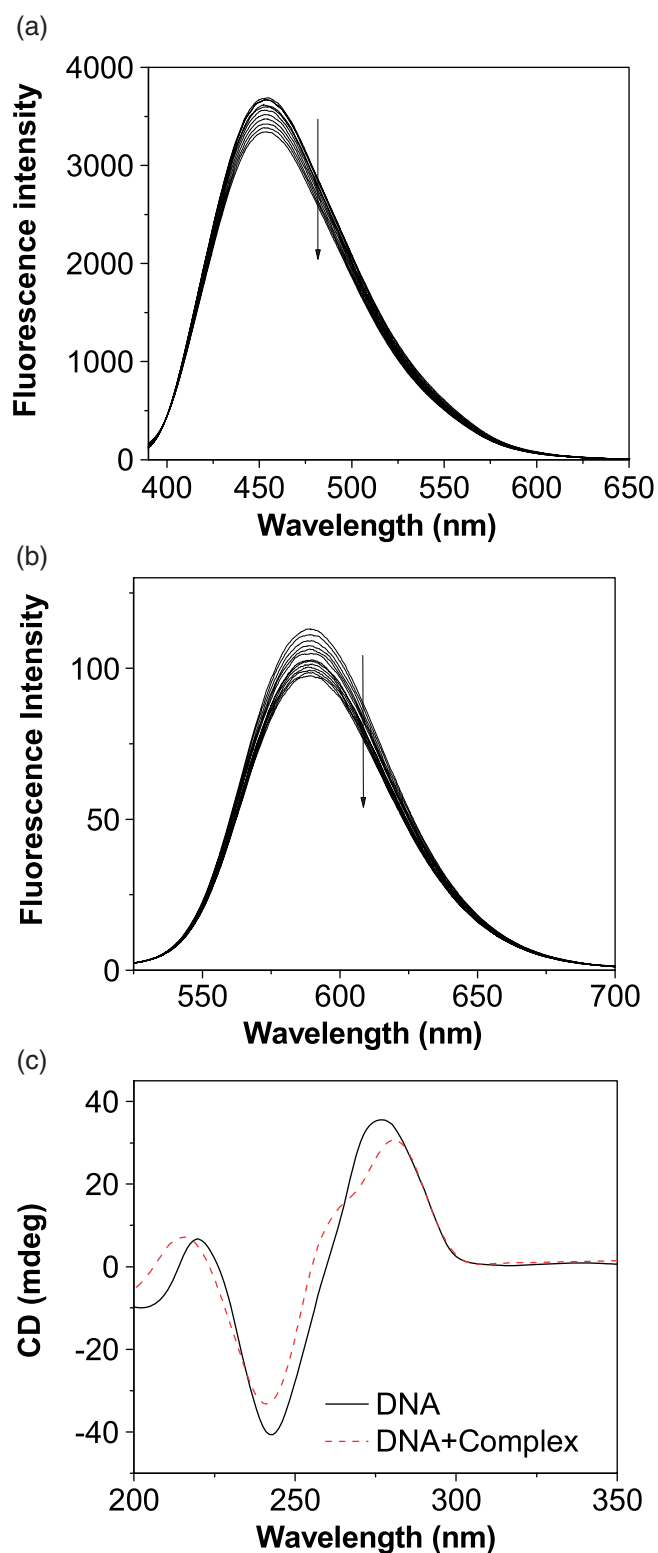


Figure 9. (a) Fluorescence titration of CT-DNA and DAPI complex with complex **1**. (b) Fluorescence titration of EtBr and ct-DNA with complex **1**. (c) CD spectra of DNA in the absence and presence of complex **1**. The concentration of [DNA] = 30 μM and [complex] = 10 μM .

that complex **1** induced a higher cytotoxicity in MCF-7 cells as compared to standard drugs (cisplatin $\text{IC}_{50} = 28 \pm 0.6 \mu\text{M}$, Morais et al., 2012). Ruthenium complexes reported earlier exhibited IC_{50} values against MCF7 cell line, $[\text{Ru}(\text{bpy})_2 \text{ p-CPIP}]^{2+}$, $\text{IC}_{50} = 64.4 \mu\text{M}$; $[\text{Ru}(\text{bpy})_2 \text{ p-NPIP}]^{2+}$, $\text{IC}_{50} = 86.5 \mu\text{M}$;

$[\text{Ru}(\text{phen})_2 \text{ p-NPIP}]^{2+}$, $\text{IC}_{50} = 38.9 \mu\text{M}$ (Perdisatt et al., 2018) in comparison to complex **1** that exhibited significantly good activity.

3.2.4. Morphological change analysis

To evaluate typical morphological changes in MCF-7 cells brought by complex **1**, cells were treated with two concentrations below IC_{50} value for complex **1** (5.0 and 10.0 μM) for 24 h. Figure 10 shows inverted microscopic images of morphological alterations observed in MCF-7 cells. The untreated control cells (Figure 10(a)) reached about 95–100% confluence contained in a typical shape and was found attached to the surface. Conversely, in the treated cells, the cells are found to lose the morphology of the normal epithelial cell, becomes elongated, and some of them found in a swelled condition. A significant decrease in cell population was observed in complex **1**-treated MCF-7 cells (Figure 10(b,c)).

3.2.5. Detection of apoptosis by flow cytometry

The percentages of early and late apoptotic and necrotic cells were measured using flow cytometry to quantify the levels of detectable phosphatidylserine on the outer membrane of apoptotic cells (Evens et al., 2004). Representative results in the form of dot plots are presented in Figure 11.

The treatment of MCF-7 with complex **1** revealed that a significant decrease ($p < 0.05$) in the population of viable cells and an increase in the percentage of apoptotic cells were observed. While in the untreated control, the only small percentage of apoptotic cells was observed (Figure 11(a)). As seen in Figure 11, when MCF-7 cells when treated with **1**, the percentage increase in the early apoptotic cells observed from 7.2% in 5.0 μM to 14.2% in 10.0 μM . whereas it late apoptotic cells decreases from 9.5 and 7.8% in 5.0 and 10.0 μM , respectively (Figure 11(b,c)).

3.2.6. Apoptotic morphological changes in MCF-7 cells

MCF-7 cells were exposed to complex **1** for 24 h as mentioned above and stained with acridine orange/ethidium bromide (AO/EB) dye to test if the increase in cell death was due to apoptosis (Figure 12).

AO/EB staining facilitates characteristic features of the apoptotic nucleus such as shrinkage of the nucleus, giving rise to fragmentation and condensation of the DNA. Around 93.7% of viable cells were prominently evident in untreated MCF-7 cells. Control cells showed a uniformly distributed green fluorescence (AO stain) with no morphological changes and no red fluorescence (Figure 12(a)). The percentage of viable cells, however, decreased significantly ($p < 0.05$) in both the treatments. As shown in Figure 12(b–d), quantification of apoptotic and necrotic cells in a total of 300 cells in each group was performed which revealed that complex **1** treatment induced the highest percentage of apoptotic cells (26.2%). The MTT assays, AO/EB staining, and flow cytometry analysis showed similar concentration and time-dependent effects on MCF-7 cells. There was a difference in the percentage of viable cells

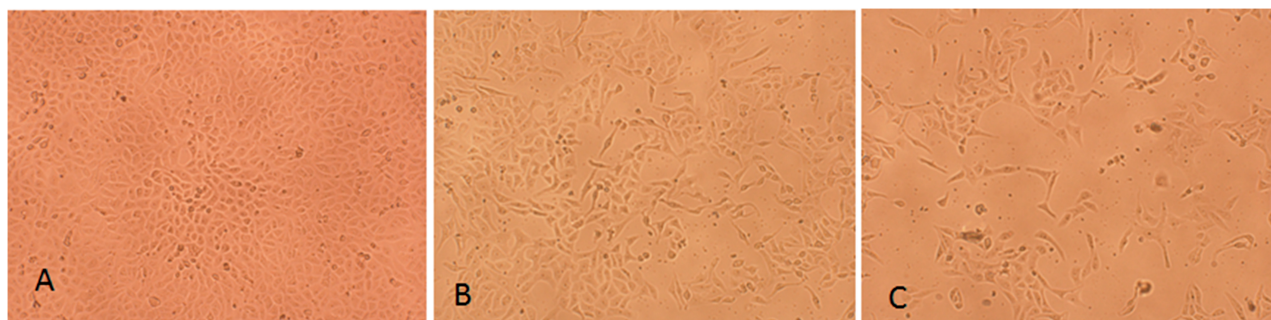


Figure 10. Phase contrast inverted microscopic observation of MCF-7 cells for morphological alterations induced by complex 1 (b,c). untreated: (a) Control; treated (b) 5.0 μM of 1 and (c) 10.0 μM of 1. Magnification: 100X.

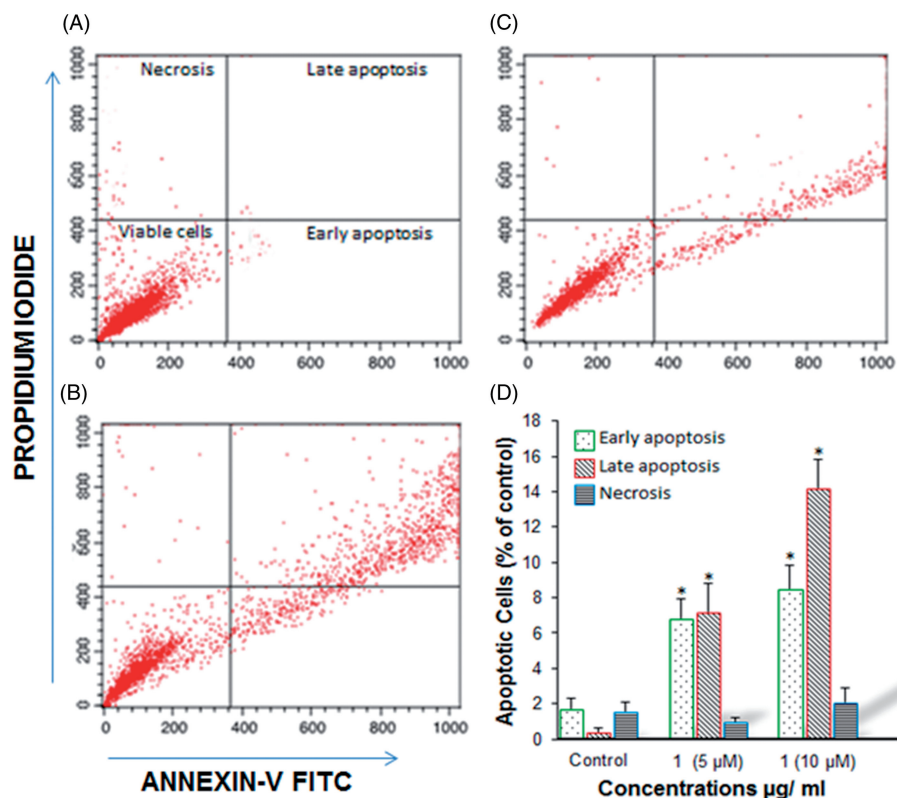


Figure 11. Flow cytometric analysis of MCF-7 cells exposed to different concentrations of complex 1 (b,c) for 24 h. Representative dot plots showing the percentage of viable cells, early apoptosis, late apoptosis, and necrotic cells: (a) control, (b) 5.0 μM , (c) 10.0 μM , and (d) bar diagrams showing the percentage of apoptosis observed by flow cytometric analysis of MCF-7 cells. All data are expressed as mean \pm SE. *Significant ($p < 0.05$) compared with controls.

because MTT is based on mitochondrial function assays that detected cell death earlier than others, while apoptosis is indicating assays (AO/EB and flow cytometry) detected cell death later in the process, which is in correlation with other reports (Ćurčić et al., 2012; Oh, Livingston, Smith, & Abrishamian-Garcia, 2004). The AO/EB method improves the detection of apoptosis and can distinguish between late apoptotic and dead cells (Liu, Liu, Liu, & Wu, 2015).

4. Conclusion

A new methodology was adopted for the search of the potential new drug with known bioactive compounds. In our studies, we have designed and synthesized a new

potential metallodrug with the use of sodium diclofenac (an anti-inflammatory drug) as bioactive ligand and coordinated it with the metal core, i.e., ruthenium(*p*-cymene) with known anticancer properties. The binding propensity of the ruthenium complex 1 with model protein (HSA) and ct-DNA was investigated. The ruthenium complex 1 binding results exhibited significant binding propensity via an interfacial binding mode. Furthermore, the ruthenium complexes were studied for cytotoxicity against MCF-7 (breast cancer cell lines), and the IC_{50} values are compared with the standard drug cisplatin, and earlier reported ruthenium complexes and ruthenium complex 1 exhibited significantly good activity. From these experimental data, we infer that the ruthenium complex 1 possesses the potential to act as an anticancer agent. The results warrant

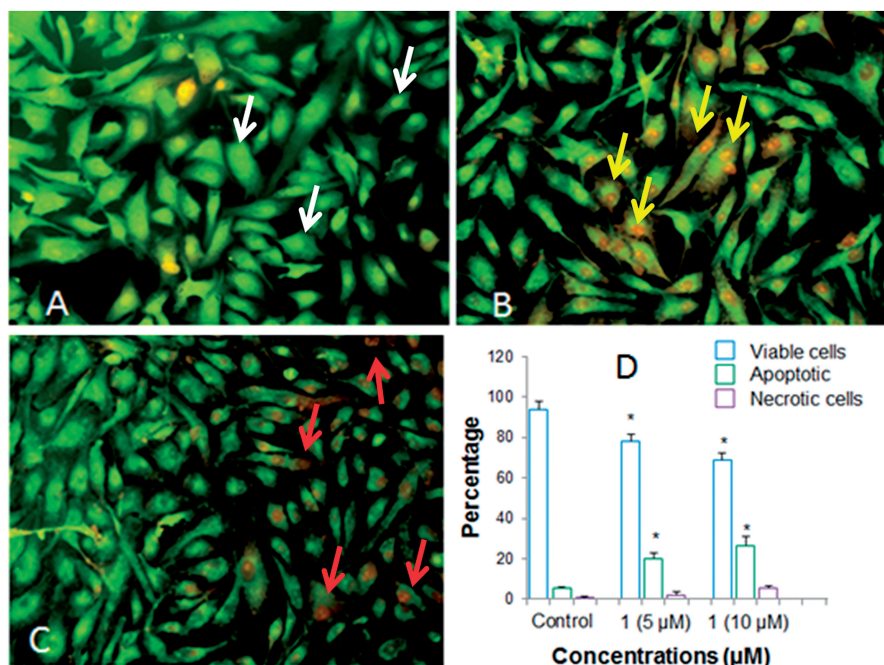


Figure 12. The Apoptotic nucleus of the MCF-7 cancerous cells are examined under fluorescence microscope. Untreated: (a) Control, Treated: (b) 5.0 μM 1, and (c) 10.0 μM 1 under 200X. (F) Quantification of cells recorded in more than 300 cells. The data is mean of \pm SE for the experiments carried out in triplicate. *Significant ($p < 0.05$) compared with control. Note: (A) Arrows indicates viable cells (living cells); (B) Arrows indicates apoptotic cells; (C) Arrows points towards necrotic cells.

further detailed investigations, and we anticipate that our findings of drug designing will contribute to the search of new anticancer drugs.

Funding

The authors are grateful to the Deanship of Scientific Research, King Saud University, for funding through Vice Deanship of Scientific Research Chairs.

References

- Afzal, M., Al-Lohedan, H. A., Usman, M., & Tabassum, S. (2018). Carbohydrate-based heteronuclear complexes as topoisomerase α inhibitor: Approach toward anticancer chemotherapeutics. *Journal of Biomolecular Structure and Dynamics*, 1–17. doi:10.1080/07391102.2018.1459321.
- Ali, M. S., & Al-Lohedan, H. A. (2013). Sulfadiazine binds and unfolds bovine serum albumin: An *in vitro* study. *Molecular Biology Reports*, 40(11), 6081–6090. doi:10.1007/s11033-013-2719-8.
- Ali, M. S., & Al-Lohedan, H. A. (2017). Deciphering the interaction of procaine with bovine serum albumin and elucidation of binding site: A multi spectroscopic and molecular docking study. *Journal of Molecular Liquids*, 236, 232–240. doi:10.1016/j.molliq.2017.04.020.
- Ali, M. S., & Al-Lohedan, H. A. (2016). Multi-technique approach on the interaction between sugar-based surfactant n-dodecyl β -D-maltoside and bovine serum albumin. *Journal of Luminescence*, 169, 35–42. doi:10.1016/j.jlum.2015.08.049.
- Anand, U., Jash, C., & Mukherjee, S. (2010). Spectroscopic probing of the microenvironment in a protein – surfactant assembly. *The Journal of Physical Chemistry B*, 114(48), 15839–15845. doi:10.1021/jp106703h.
- Aman, F., Hanif, M., Siddiqui, W. A., Ashraf, A., Filak, L. K., Reynisson, J., ... Hartinger, C. G. (2014). Anticancer ruthenium(η^6 -p-cymene) complexes of nonsteroidal anti-inflammatory drug derivatives. *Organometallics*, 33(19), 5546–5553. doi:10.1021/om500825h.
- Alsalmeh, A., Laeeq, S., Dwivedi, S., Khan, M. S., Al Farhan, K., Musarrat, J., & Khan, R. A. (2016). Synthesis, characterization of α -amino acid Schiff

- base derived Ru/Pt complexes: Induces cytotoxicity in HepG2 cell via protein binding and ROS generation. *Spectrochim, Acta A*, 163, 1–7. doi:10.1016/j.saa.2016.03.012
- Brujijninx, P. C. A., & Sadler, P. J. (2009). Controlling platinum, ruthenium and osmium reactivity for anticancer drug design. *Advances in Inorganic Chemistry*, 61, 1–62. doi:10.1016/S0898-8838(09)00201-3.
- Barry, N. P. E., & Sadler, P. J. (2013). Exploration of the medical periodic table: Towards new targets. *Chemical Communications*, 49, 5106–5131. doi:10.1039/C3CC41143E.
- Ćurčić, M. G., Stanković, M. S., Mrkalić, E. M., Matović, Z. D., Banković, D. D., Cvetković, D. M., ... Marković, S. D. (2012). Antiproliferative and proapoptotic activities of methanolic extracts from *Ligustrum vulgare*. L. as an individual treatment and in combination with palladium complex. *International Journal of Molecular Sciences*, 13(2), 2521–2534. doi:10.3390/ijms13022521.
- Evens, A. M., Prachand, S., Shi, B., Paniaqua, M., Gordon, L. I., & Gartenhaus, R. B. (2004). Imexon-induced apoptosis in multiple myeloma tumor cells is caspase-8 dependent. *Clinical Cancer Research*, 10(4), 1481–1491. doi:10.1158/1078-0432.CCR-1058-03.
- Farah, M. A., Ali, M. A., Chen, S.-M., Li, Y., Al-Hemaid, F. M., Abou-Tarboush, F. M., ... Lee, J. (2016). Silver nanoparticles synthesized from *Adenium obesum* leaf extract induced DNA damage, apoptosis and autophagy via generation of reactive oxygen species. *J. Colloids Surface B Biointerfaces*, 141, 158–169. doi:10.1016/j.colsurfb.2016.01.027.
- Feng, X. Z., Lin, Z., Yang, L. J., Wang, C., & Bai, C. L. (1998). Investigation of the interaction between acridine orange and bovine serum albumin. *Talanta*, 47(5), 1223–1229. doi:10.1016/S0039-9140(98)00198-2.
- Gasser, G., & Metzler-Nolte, N. (2012). The potential of organometallic complexes in medicinal chemistry. *Current Opinion in Chemical Biology*, 16(1–2), 84–91. doi:10.1016/j.cbpa.2012.01.013.
- Galanski, M., Arion, V. B., Jakupec, M. A., & Keppler, B. K. (2003). Recent developments in the field of tumor-inhibiting metal complexes. *Current Pharmaceutical Design*, 9(25), 2078–2089. doi:10.2174/1381612033454180.
- Hartinger, C. G., Metzler-Nolte, N., & Dyson, P. J. (2012). Challenges and opportunities in the development of organometallic anticancer drugs. *Organometallics*, 31(16), 5677–5685. doi:10.1021/om300373t.

- Hartinger, C. G., Jakupec, M. A., Zorbas-Seifried, S., Groessl, M., Egger, A., Berger, W., ... Keppler, B. K. (2008). KP1019, a new redox-active anticancer agent—preclinical development and results of a clinical phase I study in tumor patients. *Chemistry and Biodiversity*, 5(10), 2140–2155. doi:10.1002/cbdv.200890195.
- Hartinger, C. G., Zorbas-Seifried, S., Jakupec, M. A., Kynast, B., Zorbas, H., & Keppler, B. K. (2006). From bench to bedside—preclinical and early clinical development of the anticancer agent indazolium trans-[tetrachlorobis(1H-indazole)ruthenate(III)] (KP1019 or FFC14A). *Journal of Inorganic Biochemistry*, 100(5–6), 891–904. doi:10.1016/j.jinorgbio.2006.02.013.
- Hill, J. M., & Speer, R. J. (1982). Organo-platinum complexes as antitumor agents (review). *Anticancer Research*, 2(3), 173–186.
- Hudej, R., Kljun, J., Kandioller, W., Repnik, U., Turk, B., Hartinger, C. G., ... Turel, I. (2012). Synthesis and biological evaluation of the thionated antibacterial agent nalidixic acid and its organoruthenium(II) complex. *Organometallics*, 31(16), 5867–5874. doi:10.1021/om300424w
- Khan, R. A., Arjmand, F., Tabassum, S., Monari, M., Marchetti, F., & Pettinari, C. (2014). Organometallic ruthenium(II) scorpionate as topo II α inhibitor; *in vitro* binding studies with DNA, HPLC analysis and its anticancer activity. *Journal of Organometallic Chemistry*, 771, 47–58. doi:10.1016/j.jorganchem.2014.05.013
- Khan, R. A., Yadav, S., Hussain, Z., Arjmand, F., & Tabassum, S. (2014). Carbohydrate linked organotin (IV) complexes as human topoisomerase I α inhibitor and their antiproliferative effects against human carcinoma cell line (Huh7) by transcriptional regulation of specific gene. *Dalton Transactions*, 43(6), 2534–2548. doi:10.1039/c3dt51973b.
- Kelland, L. (2007). The resurgence of platinum-based cancer chemotherapy. *Nature Reviews Cancer*, 7(8), 573–584. doi:10.1038/nrc2167.
- Kljun, J., Bytzeck, A. K., Kandioller, W., Bartel, C., Jakupec, M. A., Hartinger, C. G., ... Turel, I. (2011). Physicochemical studies and anticancer potency of ruthenium η -p-cymene complexes containing antibacterial quinolones. *Organometallics*, 30(9), 2506–2512. doi:10.1021/om101180c.
- Lakowicz, J. R. (1999). *Principles of fluorescence spectroscopy* (3rd ed.). New York, NY: Springer.
- Liu, K., Liu, P. C., Liu, R., & Wu, X. (2015). Dual AO/EB staining to detect apoptosis in osteosarcoma cells compared with flow cytometry. *Medical Science Monitor Basic Research*, 21, 15–20. doi:10.12659/MSMBR.893327
- Mach, H., Volkin, D. B., Burke, C. J., & Middaugh, C. R. (1995). Ultraviolet absorption spectroscopy. In B. A. Shirley (Ed.), *Protein stability and folding: Theory and practice, methods in molecular biology* (Vol. 40, pp. 91–114). Totowa, NJ: Humana Press.
- Mandeville, J.-S., Froehlich, E., & Tajmir-Riahi, H. A. (2009). Study of curcumin and genistein interactions with human serum albumin. *Journal of Pharmaceutical and Biomedical Analysis*, 49(2), 468–474. doi:10.1016/j.jpba.2008.11.035.
- Mehta, J. V., Gajera, S. B., & Patel, M. N. (2017). Biological applications of pyrazoline-based half-sandwich ruthenium(III) coordination compounds. *Journal of Biomolecular Structure and Dynamics*, 35(7), 1599–1607. doi:10.1080/07391102.2016.1189360
- Morais, T. S., Silva, T. J. L., Marques, F., Robalo, M. P., AVECILLA, F., Madeira, P. J. A., ... Garcia, M. H. (2012). Synthesis of organometallic ruthenium(II) complexes with strong activity against several human cancer cell lines. *Journal of Inorganic Biochemistry*, 114, 65–74. doi:10.1016/j.jinorgbio.2012.04.014
- Murray, B. S., Babak, M. V., Hartinger, C. G., & Dyson, P. J. (2016). The development of RAPTA compounds for the treatment of tumors. *Coordination Chemistry Reviews*, 306, 86–114. doi:10.1016/j.ccr.2015.06.014
- Nazarov, A. A., Hartinger, C. H., & Dyson, P. J. (2014). Opening the lid on piano-stool complexes: an account of ruthenium(II)–arene complexes with medicinal applications. *Journal of Organometallic Chemistry*, 751, 251–260. doi:10.1016/j.jorganchem.2013.09.016
- Oh, H., Livingston, R., Smith, K., & Abrishamian-Garcia, L. (2004). Comparative study of the time dependency of cell death assays. *MIT Undergraduate Research Journal*, 11, 53–62.
- Perdisatt, L., Moqadasi, S., O'Neill, L., Hessman, G., Ghion, A., Qasim, M., ... O'Connor, C. (2018). Synthesis, characterisation and DNA intercalation studies of regioisomers of ruthenium (II) polypyridyl complexes. *Journal of Inorganic Biochemistry*, 182, 71–82. doi:10.1016/j.jinorgbio.2018.01.018
- Renfrew, A. K., Phillips, A. D., Egger, A. E., Hartinger, C. G., Bosquain, S. S., Nazarov, A. A., ... Dyson, P. J. (2009). Influence of structural variation on the anticancer activity of RAPTA-type complexes: PTN versus PTA. *Organometallics*, 28(4), 1165–1172. doi:10.1021/om800899e.
- Rosenberg, B., Van Camp, L., Grimley, E. B., & Thomson, A. J. (1967). The inhibition of growth or cell division in *Escherichia coli* by different ionic species of platinum(IV) complexes. *The Journal of Biological Chemistry*, 242(6), 1347–1352.
- Rosenberg, B., VanCamp, L., Trosko, J. E., & Mansour, V. H. (1969). Platinum compounds: A new class of potent antitumour agents. *Nature*, 222(5191), 385–386.
- Rosenberg, B. (1977). Noble metal complexes in cancer chemotherapy. *Advances in Experimental Medicine and Biology*, 91, 129–150.
- Rosenberg, B. (1978). Platinum complexes for the treatment of cancer. *Interdisciplinary Science Reviews*, 3(2), 134–147.
- Tabassum, S., Afzal, M., Al-Lohedan, H., Zaki, M., Khan, R. A., & Ahmad, M. (2017). Synthesis and structure elucidation of new open cubane tetranuclear [CuII₄] clusters: Evaluation of the DNA/HSA interaction and pBR322 DNA cleavage pathway. *Inorganica Chimica Acta*, 463, 142–155. doi:10.1016/j.ica.2017.04.031.
- Tabassum, S., Parveen, M., Ali, A., Alam, M., Ahmad, A., Khan, A. U., & Khan, R. A. (2012). Synthesis of novel aryl-1,2,4,5-tetrazinane-3-thiones, *in-vitro* DNA binding studies, nuclease activity and its antimicrobial activity. *Journal of Molecular Structure*, 1020, 33–40. doi:10.1016/j.molstruc.2012.03.049
- Turel, I., Kljun, J., Perdih, F., Morozova, E., Bakulev, V., Kasyanenko, N., ... Osheroff, N. (2010). First ruthenium organometallic complex of antibacterial agent ofloxacin. Crystal structure and interactions with DNA. *Inorganic Chemistry*, 49(23), 10750–10752. doi:10.1021/ic101355d.
- Usman, M., Zaki, M., Khan, R. A., Alsalmeh, A., Ahmad, M., & Tabassum, S. (2017). Coumarin centered copper(II) complex with appended-imidazole as cancer chemotherapeutic agents against lung cancer: Molecular insight via DFT-based vibrational analysis. *RSC Advances*, 7(57), 36056–36071. doi:10.1039/C7RA05874H
- Yadav, S., & Singh, J. D. (2018). Synthesis and preliminary biological evaluation for the anticancer activity of organochalcogen (S/Se) tethered chrysin based organometallic Ru^{II}(η 6-p-cymene) complexes. *Journal of Biomolecular Structure and Dynamics*, 1–40. doi:10.1080/07391102.2018.1513867.
- Yuan, C.-L., Zhang, A.-G., Zheng, Z.-B., & Wang, K.-Z. (2013). The effects of structural variations of thiophene-containing Ru(II) complexes on the acid–base and DNA binding properties. *Journal of Biomolecular Structure and Dynamics*, 31(3), 316–330. doi:10.1080/07391102.2012.698238
- Yousuf, I., Bashir, M., Arjmand, F., & Tabassum, S. (2018). Multispectroscopic insight, morphological analysis and molecular docking studies of Cu based chemotherapeutic drug entity with Human Serum Albumin (HSA) and Bovine Serum Albumin (BSA). *Journal of Biomolecular Structure and Dynamics*, 1–31. doi:10.1080/07391102.2018.1512899
- Zhang, P., & Sadler, P. J. (2017). Advances in the design of organometallic anticancer complexes. *Journal of Organometallic Chemistry*, 839, 5–14. doi:10.1016/j.jorganchem.2017.03.038